

Harnessing radiotherapy-induced NK-cell activity by combining DNA damage–response inhibition and immune checkpoint blockade

Emmanuel C Patin ¹, Magnus T Dillon,¹ Pablo Nenclares ^{1,2}, Lorna Grove,^{1,2} Heba Soliman,² Isla Leslie,² Davina Northcote,² Galabina Bozhanova,¹ Eva Crespo-Rodriguez,¹ Holly Baldock,³ Harriet Whittock,³ Gabriella Baker,¹ Joan Kyula,¹ Jeane Guevara,² Alan A Melcher,¹ James Harper,⁴ Hormas Ghadially,⁴ Simon Smith,⁴ Malin Pedersen ¹, Martin McLaughlin ¹, Kevin J Harrington ^{1,2}

To cite: Patin EC, Dillon MT, Nenclares P, *et al.* Harnessing radiotherapy-induced NK-cell activity by combining DNA damage–response inhibition and immune checkpoint blockade. *Journal for ImmunoTherapy of Cancer* 2022;**10**:e004306. doi:10.1136/jitc-2021-004306

► Additional supplemental material is published online only. To view, please visit the journal online (<http://dx.doi.org/10.1136/jitc-2021-004306>).

Accepted 06 February 2022



© Author(s) (or their employer(s)) 2022. Re-use permitted under CC BY-NC. No commercial re-use. See rights and permissions. Published by BMJ.

¹Division of Radiotherapy and Imaging, The Institute of Cancer Research, London, UK

²Head and Neck Unit, Royal Marsden Hospital NHS Trust, London, UK

³Biological Services Unit, The Institute of Cancer Research, London, UK

⁴Early Oncology R&D, AstraZeneca, Cambridge, UK

Correspondence to

Dr Emmanuel C Patin; emmanuel.patin@icr.ac.uk

ABSTRACT

Background Despite therapeutic gains from immune checkpoint inhibitors (ICI) in many tumor types, new strategies are needed to extend treatment benefits, especially in patients failing to mount effective antitumor T-cell responses. Radiation and drug therapies can profoundly affect the tumor immune microenvironment. Here, we aimed to identify immunotherapies to increase the antitumor response conferred by combined ataxia telangiectasia and Rad3-related kinase inhibition and radiotherapy.

Methods Using the human papillomavirus (HPV)-negative murine oral squamous cell carcinoma model, MOC2, we assessed the nature of the antitumor response following ataxia telangiectasia and Rad3-related inhibitor (ATRi)/radiotherapy (RT) by performing RNA sequencing and detailed flow cytometry analyses in tumors. The benefit of immunotherapies based on T cell immunoreceptor with Ig and ITIM domains (TIGIT) and Programmed cell death protein 1 (PD-1) immune checkpoint blockade following ATRi/RT treatment was assessed in the MOC2 model and confirmed in another HPV-negative murine oral squamous cell carcinoma model called SCC7. Finally, immune profiling was performed by flow cytometry on blood samples in patients with head and neck squamous cell carcinoma enrolled in the PATRIOT clinical trial of combined ATRi/RT.

Results ATRi enhances radiotherapy-induced inflammation in the tumor microenvironment, with natural killer (NK) cells playing a central role in maximizing treatment efficacy. We demonstrated that antitumor activity of NK cells can be further boosted with ICI targeting TIGIT and PD-1. Analyses of clinical samples from patients receiving ATRi (ceralaseritib) confirm the translational potential of our preclinical studies.

Conclusion This work delineates a previously unrecognized role for NK cells in the antitumor immune response to radiotherapy that can be augmented by small-molecule DNA damage–response inhibitors and immune checkpoint blockade.

INTRODUCTION

Head and neck squamous cell carcinomas (HNSCCs) have an annual global incidence of approximately 750 000 cases with a mortality rate of around 50%.¹ Classical risk factors are smoking, alcohol consumption, and human papillomavirus (HPV) infection. Surgery and/or radiotherapy/chemoradiotherapy are standard-of-care curative treatments in HNSCC. They are, however, associated with severe treatment-related morbidity and, in a significant proportion of patients, are ineffective at preventing locoregional recurrence and metastatic disease, which are the major causes of mortality.² There is an urgent need for the development of effective, well-tolerated treatments that deliver durable locoregional and systemic disease control.

Radiotherapy induces the DNA damage response (DDR),³ which involves processes that sense DNA damage, induce cell cycle arrest, and attempt DNA repair to restore normal DNA sequence.⁴ Ataxia telangiectasia and Rad3-related (ATR) kinase is critical for replication fork stability in response to replication stress or radiation-induced DNA damage.⁵ Ataxia telangiectasia and Rad3-related inhibitors (ATRi) have shown promising clinical results as monotherapy particularly in tumors with ATM deficiency and have demonstrated radiosensitization in preclinical models.^{6–8}

There is an emerging consensus that the DDR pathway defects or pharmacological inhibition can promote antitumor immune responses. Mechanistically, this is due to micronucleus generation, sensing of cytosolic DNA by cyclic GMP-AMP Synthase

- Stimulator of Interferon Genes (cGAS-STING) and subsequent type I interferon (IFN) production.^{9 10} Our group and other groups have shown that combinations of radiation and AZD6738 reduce tumor burden and modulate the tumor immune microenvironment (TIME), with increased lymphocyte and myeloid cell infiltration in *in vivo* models.^{11 12} The efficacy of AZD6738, as monotherapy or combined with radiotherapy, is currently under clinical evaluation.¹³

Immune checkpoint inhibitors (ICIs) exert significant activity as single agents or in combination with cytotoxic chemotherapy in patients with relapsed/metastatic HNSCC.^{14–16} However, initial attempts to combine anti-programmed cell death protein 1 (PD-1) immune checkpoint inhibitors (ICI) and radiotherapy/chemoradiotherapy as curative treatments for locally advanced HNSCC have not delivered improvements on standard-of-care regimens.¹⁷ This failure may be due, at least in part, to the empirical, one-size-fits-all approach of simply adding anti-PD-1/anti-programmed death-ligand 1 (PD-L1) ICIs to current regimens, without any attempt at biomarker-led or mechanism-based patient selection. We posited that combining radiotherapy, DNA damage response inhibitors (DDRi) and ICIs might represent a rational approach to developing new therapeutic strategies derived from detailed preclinical analyses in relevant immunocompetent animal models.

Therefore, we have sought to understand how changes in tumor-infiltrating leukocytes that occur following radiation and AZD6738 combination therapy can be exploited to maximize therapeutic benefits. Here, using syngeneic mouse models of head and neck cancer, we confirm the profound impact of radiation and ATRi combination therapy on the TIME. We identify natural killer (NK) cells as critical players in mediating optimum treatment efficacy and show that their activity can be boosted with mechanistically appropriate ICI. In confirmatory studies, immune profiling of clinical samples supports the relevance of our findings to human cancers and points the way toward clinical translation.

MATERIALS AND METHODS

Human studies

Blood samples were taken from patients enrolled on the phase I PATRIOT study of Ceralasertib (AZD6738) in combination with palliative radiotherapy (EudraCT: 2013-003994-84). Patients were 18 years and over, with a diagnosis of advanced solid malignancy and an indication for palliative radiotherapy. All patients had an Eastern Cooperative Oncology Group performance status of 0–2 with a life expectancy of at least 3 months and adequate organ function. Radiotherapy was administered daily, 2 Gy per fraction, Monday–Friday. A total of 30 Gy in 15 fractions was administered. Ceralasertib was administered orally at a dose of 80 mg (the recommended phase II dose), two times per day, for 3–7 days before the start of radiotherapy, during radiotherapy, and for 2 days after.

Blood was taken before ceralasertib dosing, before fraction 1, before fraction 6, and before fraction 11, in an 8 mL EDTA tube and was processed within 24 hours of sampling.

Mouse models of head and neck cancer

Female C57BL/6 and C3H mice 8–14 weeks old were purchased from Charles River and allowed to acclimate to the Institute of Cancer Research (ICR) animal facility for a week. All animals were handled according to the Institute of Cancer Research and UK Home Office guidelines. In this study, we used three different models of murine immunocompetent HPV-negative head and neck cancer. The C57BL/6 mouse cancer cell line MOC2 was kindly provided by Ravindra Uppaluri (Dana-Farber Cancer Institute). The C3H mouse HPV-negative cancer cell lines AT-84 and SCC7 cells were kindly provided by Laird Forrest (University of Kansas) and Richard Vile (Mayo Clinic), respectively. Cells were cultured and maintained in Dulbecco Modified Eagle Serum supplemented with 10% fetal calf serum (FCS), 2 mM L-glutamine, penicillin/streptomycin, and sodium pyruvate. Mice were inoculated subcutaneously on the right or left flank as indicated with 2×10^6 cells for both MOC2 or AT-84 models or 10^6 cells for the SCC7 model. Tumor growth was monitored every 3/4 days using a caliper and expressed as volume ($(\text{length} \times \text{width} \times \text{depth})/2$). Mice were euthanized when tumors reached an average of 15 mm in two of the three dimensions.

In vivo tumor treatments

In vivo treatment was initiated when tumors reached an average of 50–200 mm³. The ATRi AZD6738 was provided by AstraZeneca and solubilized in 10% dimethyl sulfoxide (DMSO), 40% propylene glycol, 50% water, orally administered 2 hours before irradiation for 5 or 7 consecutive days at 25 or 75 mg/kg/dose as indicated. Animal tumors were irradiated under anesthesia with Hypnorm and Hyprovel injected intraperitoneally. Irradiation was performed using an AGO 250 kV X-ray machine at a dose rate of 1.62 Gy/min (AGO). Animals were irradiated in the prone position and positioned under lead shielding with a 16 mm diameter aperture aligned over the tumor. A total of 8–24 Gy radiation dose in three to four fractions was given as indicated. Radiation dose was measured using a Farmer Chamber and Unidos-E Dosemeter (both PTW). When indicated, mice were treated with anti-TIGIT (clone 1G9) and/or anti-PD-1 (clone RMPD1-14) antibodies from BioXcell. Both antibodies were injected at a dose of 200 µg/mouse intraperitoneally, two times per week for 3 weeks, the first injection administered just after the last radiation dose. For the depletion of NK cells, mice were injected intraperitoneally with 200 µg/mouse of anti-NK1.1 antibody (BioXcell, clone PK136) or 50 µL/mouse anti-Asialo-GM1 (BioLegend, clone Poly21450) into C57BL/6 mice or C3H mice, respectively, two times per week starting 1 day before treatment. For the depletion of CD8 T cells, mice were injected intraperitoneally

with 200 µg/mouse of anti-CD8α (BioXcell, clone 2.43) two times per week starting 1 day before treatment.

Cytokine detection by ELISA

Tumors from MOC2-bearing mice were harvested 4 days after the last radiation dose and 1 day after the last ATRi dose. Tumors were weighted and collected in cold PBS until processing. Tumors were then homogenized in 1 mL PBS. Tubes were centrifuged and supernatants were collected for ELISAs. Detection of cytokines was performed using interferon gamma (IFN-γ), interferon beta (IFN-β) and interleukin (IL)-10 (R&D Systems) ELISA kits following the manufacturer's instructions. Data were normalized with tumor weights.

RNA sequencing (RNA-seq)

MOC2 tumors were harvested 3 and 10 days after the last radiation dose. RNA from tumors was extracted and purified from tumors using the NucleoSpin RNA extraction kit (Macherey-Nagel). Library preparation and sequencing were performed by Genewiz (Leipzig, Germany). Library prep was strand-specific, used PolyA selection, with 2×150 bp sequencing at 10 million pairs performed on an Illumina NovaSeq. Quality control was performed using FastQC. Low-quality bases and adaptor sequences were removed using Trimmomatic. Reads were mapped to the *Mus musculus* GRCm38 reference genome using HISAT2, samtools and StringTie. Differential gene expression was assessed using DESeq2. Enrichment analysis for Gene Ontology terms was performed on differentially expressed genes (DEGs) using topGO. Active subnetwork-orientated gene set enrichment analysis using STRING protein-protein interaction networks and Kyoto Encyclopedia of Genes and Genomes pathways was performed using pathfindR. Immune cell composition was estimated from transcriptomic data using murine microenvironment cell population (mMCP)-counter. Data visualization used ggplot2 and ComplexHeatmap packages.

Flow cytometry analysis

Harvested tumors were excised, finely minced, and enzymatically digested for 30–45 min at 37°C in PBS containing 1 mg/mL collagenase type VI (Sigma-Aldrich), 1 mg/mL DNase type I (Roche), 100 ng/mL Dispase (Sigma-Aldrich), and trypsin. Digested tumors were smashed and filtered through a 70 µm pore cell strainer. Cells were centrifuged at 1400 rpm at 4°C for 10 min and pellets were washed in PBS/2% FCS/5 mM EDTA. Harvested spleen were mechanically dissociated, smashed, and filtered through a 70 µm pore cell strainer. Red blood cells were lysed by a 1 min incubation in ACK lysis buffer (Thermo Fisher Scientific). Cells were centrifuged at 1400 rpm at 4°C for 10 min and pellets were washed in PBS/2% FCS. For some experiments, mice were bled 20 µL from the tail vein. PBMCs from human blood samples were isolated on a density gradient medium (Lymphoprep, STEMCELL Technologies). Cells were incubated

4°C for 10 min with anti-mouse or anti-human CD16/CD32 (BD Pharmingen) prior to surface staining, 4°C for 30 min. The complete list of antibodies used in this study can be found in the online supplemental information. Intranuclear detection of Ki67 was performed using The Foxp3 Transcription Factor Staining Buffer Set (Thermo Fisher Scientific) following the manufacturer's instructions. For intracellular cytokine detection and surface detection of CD107a, cells were incubated in complete IMDM containing Golgi Plug/Golgi Stop (BD Biosciences) in the presence of a stimulation cocktail containing PMA and ionomycin (Invitrogen) and mouse CD107a antibody for 4 hours at 37°C. Following surface antibody staining, cells were fixed using IC fixation buffer (Invitrogen), permeabilized in permeabilization buffer (Invitrogen), and stained with mouse IFN-γ antibody. Samples were analyzed on an LSR II or FACSymphony A5 (BD Biosciences), and flow cytometry (FACS) analyses were performed using the FlowJo V.10 software.

Statistical methods

Statistical analysis were performed using GraphPad Prism software V.8 and V.9. Data are presented as means±SEM and are from a single or cumulative of two to three independent experiments. Areas under the curve were used to determine statistical differences in tumor growth between groups. Statistical differences between survival groups were determined using the log-rank Mantel-Cox test. Intensity of marker expression was shown as geometrical mean fluorescence intensity in the positive population. Unpaired t-test or one-way analysis of variance (ANOVA) followed by Tukey's post t-test was used for statistical analysis when two or multiple groups were analyzed, respectively. When data did not follow a Gaussian distribution, we used non-parametric Mann-Whitney U or Kruskal-Wallis test followed by Dunn's post-t-test for statistical analysis when two or multiple groups were analyzed, respectively. We used two-way ANOVA when multiple parameters were studied. Significant outliers were removed using the Grubb test. Statistical significance was assumed with *p<0.05, **p<0.005, ***p<0.001, and ****p<0.0001.

RESULTS

Combination of radiotherapy and ATR inhibition induce an antitumor response in head and neck cancer models

First, we evaluated the potential benefit of combining ATRi/RT in vivo using two murine oral squamous cell carcinoma models, MOC2 and AT84. Tumor-bearing mice were treated with conventionally fractionated RT, ATRi, or the combination (figure 1A).

MOC2 and AT84-bearing mice (figure 1B and online supplemental figure S1, respectively) displayed a marked reduction in tumor burden and significantly increased survival rates following ATRi/RT treatment when compared with control or single agents. To address whether an immune response was induced, we analyzed cytokine production in tumors following combination

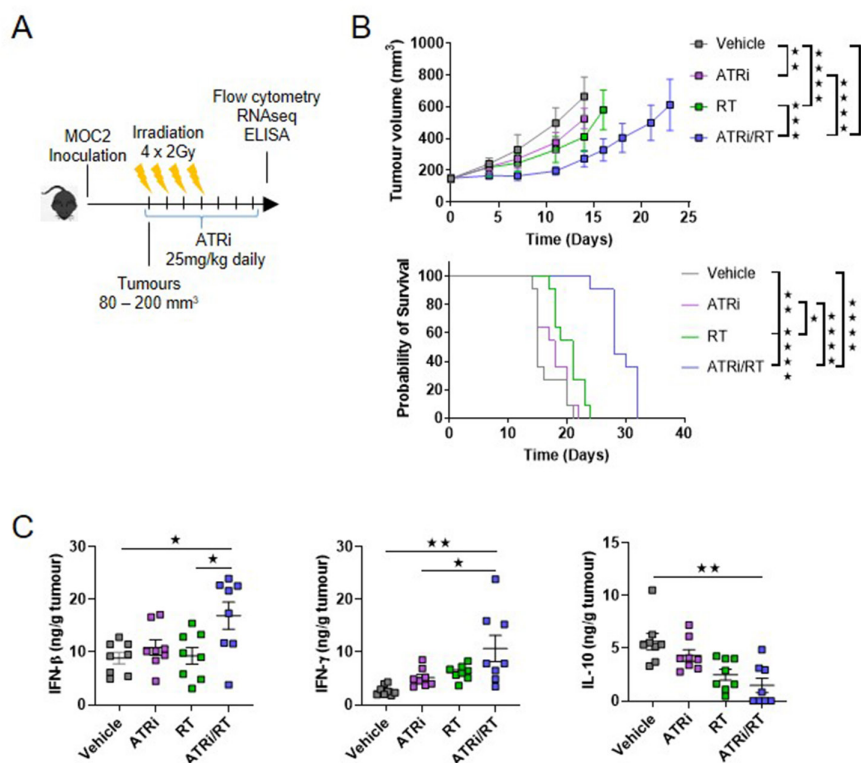


Figure 1 ATRi potentiates RT-mediated antitumor immune response. (A) Experimental design for the treatment of MOC2 tumors. 2×10^6 MOC2 cells were injected subcutaneously into C57BL/6 mice. When tumors reached 80–200 mm³, mice were treated with ATRi (25 mg/kg/day for 7 days) and RT (8 Gy in four 2 Gy/day fractions) at time as indicated. Primary tumor growth was monitored every 3 days to 4 days. (B) Combined tumor growth and survival curves from two independent experiments are shown (11 mice/group). (C) IFN- β , IFN- γ , and IL-10 cytokine concentration determined in tumor homogenates by ELISA and normalized with tumor weights (eight mice/group). Results are shown as \pm SEM, one-way analysis of variance followed by Bonferroni's post-t-test. Statistical differences between survival groups were determined using the log-rank Mantel-Cox test. Statistical significance: * $p < 0.05$, ** $p < 0.01$, *** $p < 0.001$, **** $p < 0.0001$. ATRi, ataxia telangiectasia and rad3-related inhibitor; IFN- β , interferon beta; IFN- γ , interferon gamma; IL, interleukin; RT, radiotherapy.

therapy. We observed a significant increase in IFN- β and IFN- γ production in response to ATRi/RT when compared with control (figure 1C). Interestingly, this was paralleled by a decrease in IL-10 production, which supports the induction of a strong proinflammatory response in the TIME (figure 1C).

Together, these data indicate a beneficial effect of ATRi in combination with RT in two different head and neck cancer models. Cytokine production analysis after the combination therapy also suggests the involvement of the immune system in this treatment effect.

ATRi and radiotherapy induce a gene expression profile characteristic of NK-cell activity

To determine the nature of the antitumor response following ATRi/RT, we performed RNA-seq in MOC2 tumors on days 3 and 10 postirradiation. Principal component and differential gene expression analyses showed significant changes induced by ATRi and RT, with biological replicates clustering together (online supplemental figure S2). The number of DEGs was higher at day 3 in the combination therapy when compared with individual therapies (figure 2A). At day 10, a higher number of DEGs were observed for ATRi alone (figure 2A).

Enrichment analysis for gene ontology terms linked to DEGs revealed the majority of treatment-induced changes appeared at day 3 (figure 2B, online supplemental table S1). Significant enrichment in all treatment groups was identified for the ontology terms response to bacterium, negative regulation of viral genome replication, cellular response to IFN- β , and defense response to virus (figure 2B), indicative of a viral mimicry signature. Enrichment for the ontology terms cytolysis, innate immune response, and stimulatory C-type lectin receptor signaling pathway was observed only in the ATRi/RT combination group (figure 2B). These ontology terms are rich in NK cell-associated transcripts. At day 10, most of the ontology groups mentioned at day 3 had returned to baseline except for cellular response to IFN- β and cytolysis in the case of ATRi/RT. As variations of gene expression were mostly detected at day 3, we focused on this timepoint in further analyses. Parallel pathway analysis of DEGs using the pathfindR package at day 3 showed significance for hepatitis C-associated, influenza A-associated, and measles-associated gene signatures in all groups when compared with control (figure 2C). These pathway terms are linked by IFN-stimulated genes

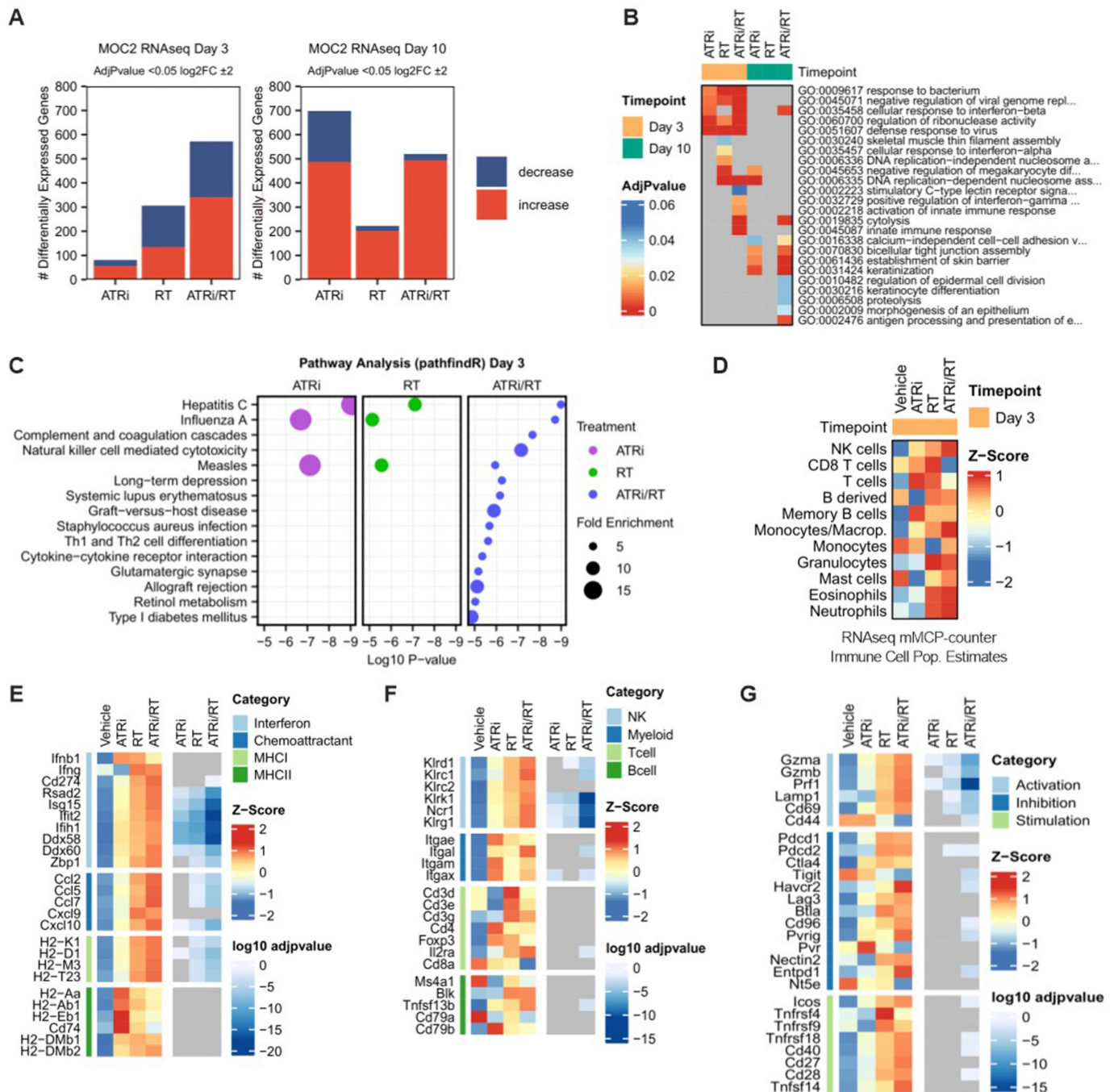


Figure 2 MOC2 RNA-seq analyses indicate an NK-cell innate immune phenotype in response to ATRi/RT. MOC2 tumor-bearing mice were treated as previously described in figure 1. Tumors were collected at days 3 and day 10 post-RT for RNA-seq. (A) The number of DEGs at days 3 and day 10 post-RT compared with vehicle at each timepoint calculated by DESeq2. (B) Gene set enrichment analysis for gene ontology terms linked to the DEGs identified using the TopGO package. Non-significant adjusted p values of >0.05 are indicated as gray. (C) Pathway analysis of DEGs at day 3 using the pathfindR package. The absence of a plotted datapoint indicates that the pathway listed is non-significant under that treatment. (D) Immune cell population estimates at day 3. Immune cell scoring was performed on normalized RNA-seq counts using the mMCP-counter package. Heatmaps corresponding to interferon and cytokine signaling (E), immune cell populations (F), and immune cell activation status (G). Data shown are z-scores of log₂-transformed normalized counts at day 3 for the treatment conditions shown. This is plotted alongside log₁₀ adjusted p value for each gene calculated from DEG analysis using DESeq2. Non-significant adjusted p values of >0.05 are indicated as gray. ATRi, ataxia telangiectasia and rad3-related inhibitor; DEG, differentially expressed gene; NK, natural killer; RNA-seq, RNA sequencing.

(online supplemental table S2) that, again, reflect a viral mimicry signature. Strikingly, broad upregulation of a number of pathways was seen in response to ATRi/RT,

including NK cell-mediated cytotoxicity, graft-versus-host disease, allograft rejection and type I diabetes mellitus (figure 2C). Therefore, gene ontology and pathfindR

analyses both independently highlighted terms linked to NK-cell activity.

Immune cell population estimates highlighted the prominence of NK cells, monocytes, macrophages, and granulocytes (including eosinophils and neutrophils), but not CD8 T cells, in MOC2 tumors in response to ATRi/RT (figure 2D). In line with previous data, analyses of transcripts of individual genes revealed that the ATRi/RT combination significantly induced IFN signaling, chemoattractant and MHCI-related genes (figure 2E). In terms of immune cell population gene signatures, the most strikingly significant p values were observed for NK-cell receptors, such as *Klrk1*, *Ncr1*, and *Klrg1* in response to ATRi/RT (figure 2F). We also detected, in the same treatment group, a marked increase in gene expression for immune cell activation markers, especially granzymes and perforin (figure 2G), which was sustained until day 10 post-treatment (online supplemental figure S3). Finally, consistent with an NK-cell gene signature, we found a marked increase in the expression of genes important for their activity, such as *Ili2b*, *Ili5*, *Ili5ra*, and *Ili8* (online supplemental figure S4).

Taken together, RNA-seq analyses suggest that ATRi/RT combination therapy triggers a robust innate immune response likely to be mediated by the activity of NK cells.

ATRi and radiotherapy trigger an NK cell-mediated antitumor immune response

To confirm RNA-seq findings and define the cellular components of the immune system responsible for ATRi/RT-mediated antitumor activity, MOC2 tumors were analyzed with a focus on lymphocyte populations (gating strategy shown in online supplemental figure S5). We observed a decrease in the proportions of both CD4 and CD8 T cells in total immune cell infiltrates (live CD45⁺ cells) (figure 3A). The distribution of $\gamma\delta$ and other T-cell populations was not affected. The combination of ATRi/RT enhanced the proportion of NK cells to a greater extent than single treatment regimens (figure 3A). The increased frequency of NK cells was even more pronounced when reported relative to the lymphocyte compartment (figure 3B). Studies on the myeloid cell compartment only showed significant variations in monocyte infiltrates (online supplemental figure S6).

Next, we determined the functional importance of NK cells to the therapeutic efficacy of ATRi/RT combination therapy. We compared MOC2 tumor growth in mice treated with ATRi/RT in the presence or absence of NK cells using specific depleting antibodies. While treatment efficacy was significantly decreased in the absence of NK cells (figure 3C), a similar experiment with a CD8-depleting antibody showed no involvement of CD8 T cells (figure 3D). This was despite efficient intratumoral depletion of both NK cells and CD8 T cells in tumors (online supplemental figure S7).

These data suggest that the accumulation of NK cells in the TIME plays a significant role in the efficacy of ATRi/RT combination therapy.

Combination of radiation and ATRi therapy increases NK-cell activation in the TIME

In line with data on the impact of NK-cell depletion, we investigated whether ATRi/RT administration induced an increase of the maturation/activation of NK cells in the TIME. We observed enhanced maturation of tumor-infiltrating NK cells as higher frequencies of CD11b⁺/CD27⁻ cells on ATRi/RT treatment when compared with the control group (figure 3E). We noted a marked increase in the proportion of NK cells expressing activation/memory/proliferation markers, such as CD69, CD44, NKG2D, and Ki67, as well as the costimulatory molecule 4-1BB (figure 3F). We assessed whether the increased NK-cell activation detected in the tumor bed was accompanied by greater effector and killing capacities. Therefore, we analyzed intracellular IFN- γ staining and surface expression of the degranulation marker CD107a (LAMP-1) in intratumoral NK cells on ex vivo stimulation. We observed that radiotherapy and ATRi combination therapy strongly increased the frequencies of both IFN- γ and CD107a-positive NK cells (figure 3G).

Taken together, these results demonstrate that ATRi/RT combined treatment significantly boosts the activity of NK cells in the TIME, making them an interesting target for immunotherapies.

ATRi and radiation create a TIME suitable for modulation by immune checkpoint blockade

Next, we aimed to identify therapeutic strategies to increase the antitumor response conferred by ATRi/RT treatment. We hypothesized that immune checkpoint blockade could further boost the activity of NK cells in the TIME.

Thus, we addressed whether ATRi/RT increased or curbed surface expression of various immune checkpoint molecules on tumor-infiltrating NK cells. Although RNA-seq showed a significant decrease in its total gene expression (figure 2F), our results revealed that, among the various immune checkpoints studied, expression of TIGIT alone was enhanced on the surface of intratumoral NK cells after ATRi/radiation treatment when compared with control (figure 4A). Of note, TIGIT expression on the surface of CD4 T cells was slightly reduced and no variation was detected on CD8 T cells (online supplemental figure S8). We also observed a decrease in the frequencies of both PD-1 and CTLA-4-positive NK cells, whereas the frequencies of those expressing TIM-3, LAG-3, NKG2A, CD96 (tactile), or KLRG1 were unchanged (figure 4A). Interestingly, among the total TIGIT⁺ NK-cell population, matured CD11b⁺/CD27⁻ NK cells were dominant (figure 4B).

Concerning the expression of immune checkpoint ligands in tumors, we detected higher proportions of cancer and myeloid cells (macrophages and monocytes) expressing one of the TIGIT ligands, namely, poliovirus receptor (PVR/CD155) (figure 4C). This provided further assurance that the TIGIT/PVR axis could serve as a relevant therapeutic target. Immune checkpoint

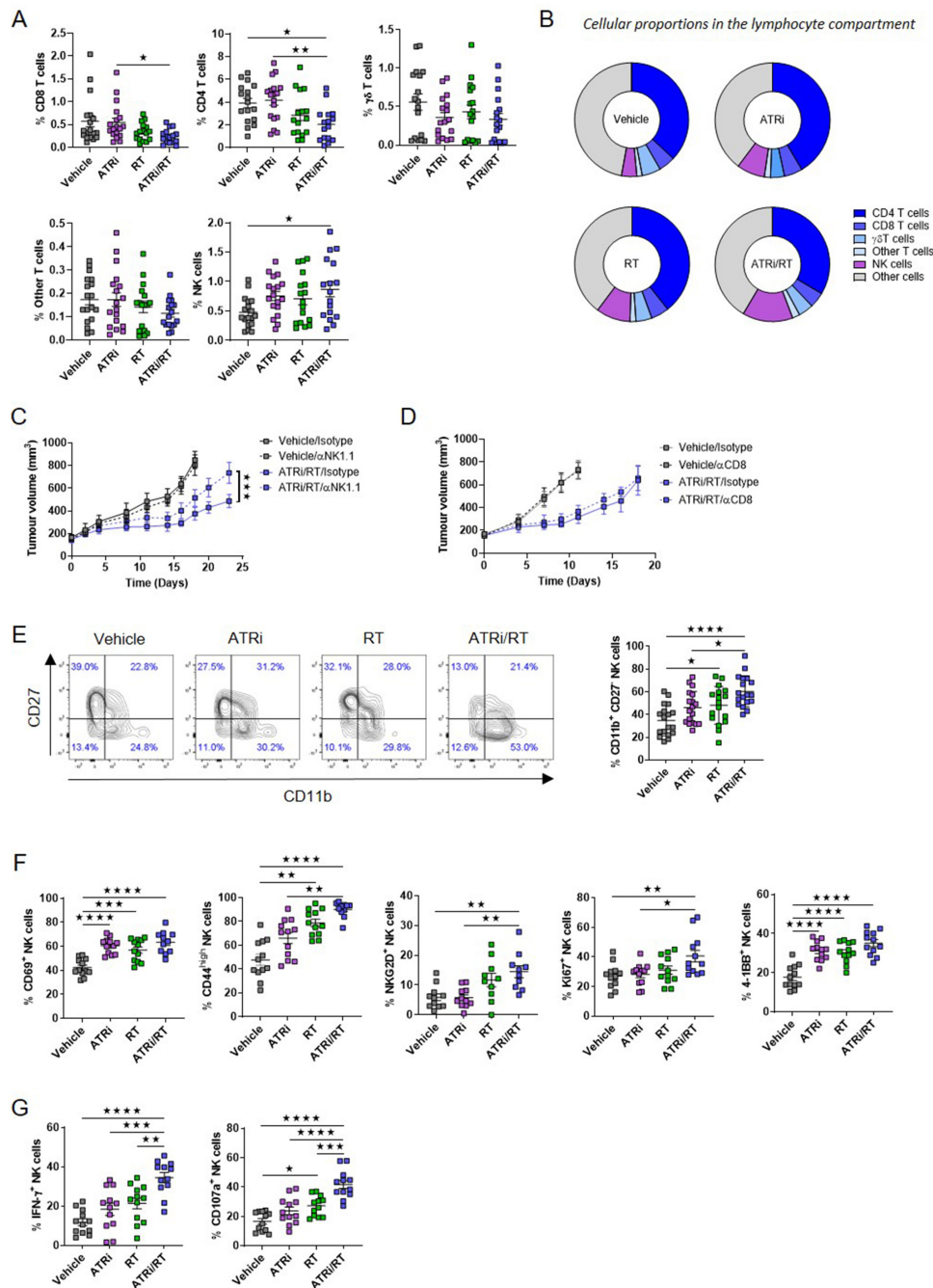


Figure 3 ATRi/RT combination treatment promotes antitumor immune response through NK-cell activity. (A) MOC2 tumor-bearing mice were treated with ATRi/RT combination therapy as previously described. Tumors were collected 1 day after the last ATRi dose for flow cytometry analysis. Cell subset proportions in total live CD45⁺ cells were compared between each group. Combined percentages from three independent experiments are shown (17–18 mice/group). (B) Cell subset proportions in total lymphocytes represented on pie charts. Combined data from three independent experiments are shown (17–18 mice/group). (C,D) MOC2 tumor-bearing mice were treated with ATRi/RT combination therapy. NK cells (C) or CD8 T cells (D) were depleted in the indicated group using an anti-NK1.1 or anti-CD8 α antibody, respectively. Combined tumor growth and survival curves from two (C) and one (D) independent experiments are shown (six to eight mice/group). (E) NK-cell maturation in response to ATRi and/or RT combination treatment as shown by surface expression of CD11b and CD27. Dot plot concatenate from 6 mice for each group (left panel) and combined percentages (right panel) from three independent experiments (17–18 mice/group). (F) Frequencies of intratumoral NK cells expressing CD69, CD44, NKG2D, Ki67, and 4-1BB shown as combined percentages from two independent experiments (11–12 mice/group). (G) Cytokine production and degranulation capacity of intratumoral NK cells as shown by the proportion of IFN- γ and CD107a-positive cells. Combined data from two independent experiments are shown (12 mice/group). Results are shown as \pm SEM, one-way analysis of variance followed by Bonferroni's post-t-test. Statistical differences between survival groups were determined using the log-rank Mantel-Cox test of statistical significance: * $p < 0.05$, ** $p < 0.01$, *** $p < 0.001$, **** $p < 0.0001$. ATRi, ataxia telangiectasia and rad3-related inhibitor; IFN- γ , interferon gamma; NK, natural killer.

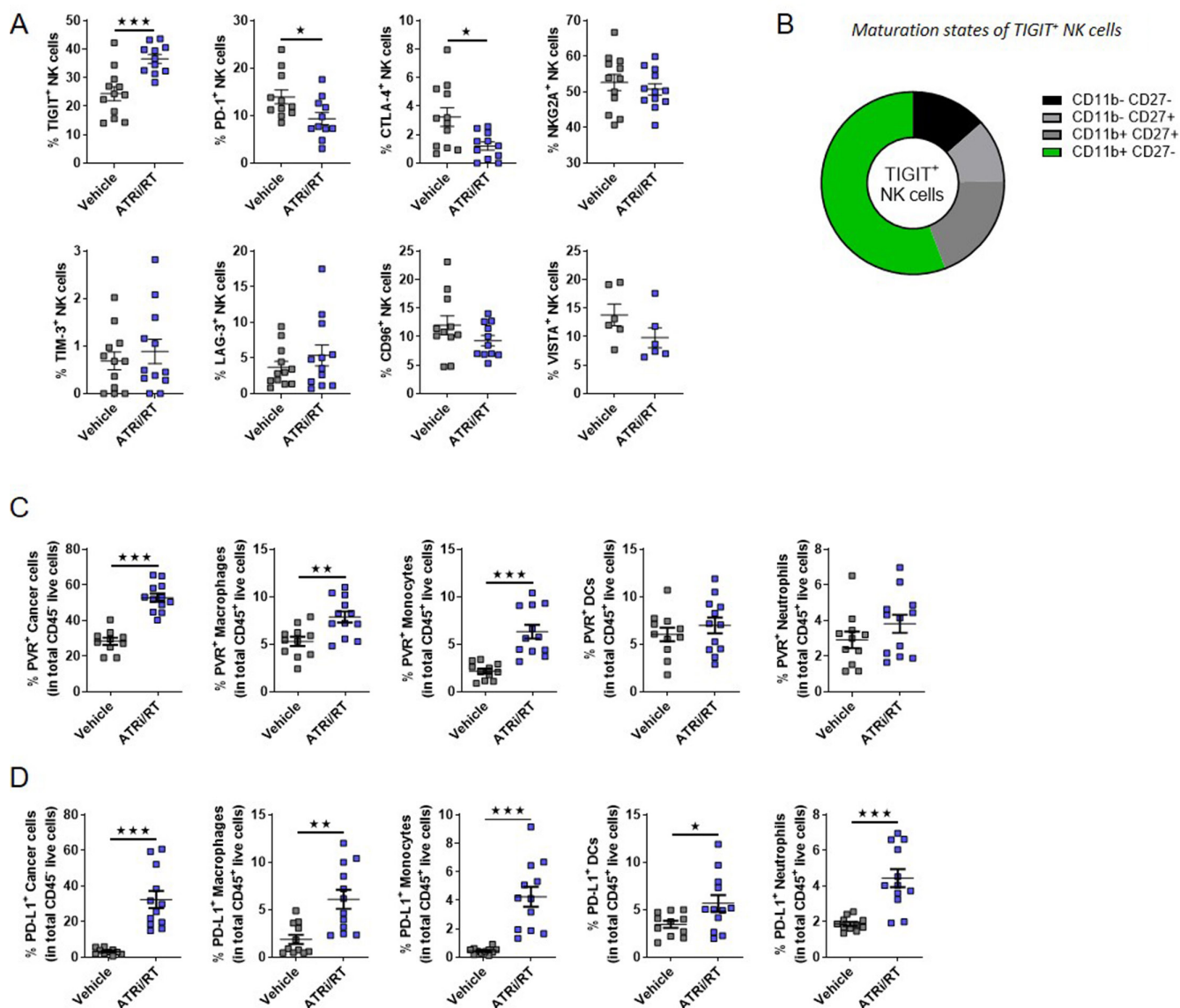


Figure 4 ATRi/RT combination therapy increases the frequencies of TIGIT-positive NK cells and PVR and/or PD-L1-positive cancer and myeloid cells in the tumor microenvironment. (A) Percentages of MOC2 tumor NK cells expressing indicated immune checkpoints following ATRi/RT combination therapy as previously described (6–12 mice/group). (B) Maturation stages of TIGIT⁺ versus TIGIT⁻ NK cells as determined by the surface expression of CD11b and CD27 markers (means for six mice/group). Percentages of PVR and PD-L1-positive cancer and myeloid cells in MOC2 tumors following ATRi/RT combination therapy as previously described (12 mice/group). Results are shown as \pm SEM, unpaired t-test for data following Gaussian distribution, Mann-Whitney U test for data not following Gaussian distribution. Statistical significance: *p<0.05, **p<0.01, ***p<0.001. ATRi, ataxia telangiectasia and rad3-related inhibitor; NK, natural killer; PVR, poliovirus receptor.

antagonists, such as PD-1/PD-L1 antibodies, are approved to treat patients with head and neck cancer.¹⁸ Therefore, although the proportion of PD-1-positive NK cells declined in the TIME on treatment, we tested whether PD-L1 expression would follow an opposite trend and provide a rationale for using anti-PD-1/PD-L1 axis-blocking agents to improve ATRi/RT in MOC2 tumor-bearing mice. We noted a striking increase in PD-L1 expression on cancer cells and intratumoral myeloid cells in response to combination therapy (figure 4D).

Collectively, these results provide the rationale to combine TIGIT and/or PD-1-blocking antibodies with

ATRi/RT treatment in order to unleash NK-cell activity in the TIME.

Combined blockade of TIGIT and PD-1 improves ATRi/RT-mediated tumor control

MOC2 tumor-bearing mice were treated with anti-TIGIT and/or anti-PD-1-blocking antibodies in addition to ATRi/RT. Systemic administration of anti-TIGIT and PD-1 antibodies significantly improved ATRi/RT treatment in terms of both tumor growth and tumor-specific survival (figure 5A). The concomitant combination of

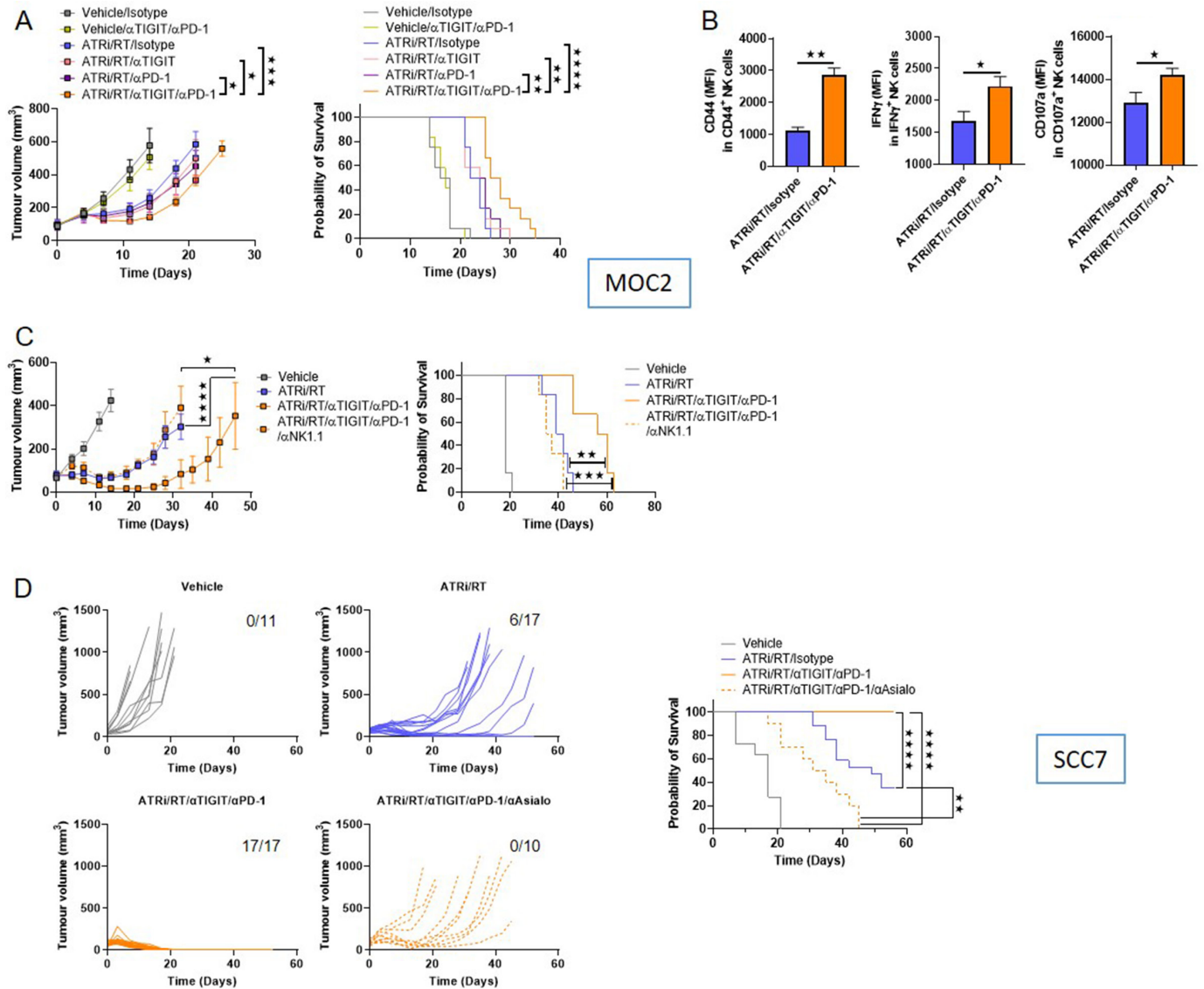


Figure 5 Combined blockade of TIGIT and PD-1 improves ATRi/RT combination therapy in two human papillomavirus-negative mouse models of head and neck squamous cell carcinoma. (A) MOC2 tumor-bearing mice were treated with ATRi/RT combination therapy as previously described. After the last radiation dose, mice were treated with anti-TIGIT and/or anti-PD-1 antibodies two times per week for 3 weeks. Combined tumor growth and survival curves from two independent experiments are shown (12 mice/group). (B) Expression of CD44, IFN- γ and CD107a in intratumoral NK cells as shown by MFI in the positive population (six mice/group). (C) MOC2 tumor-bearing mice were treated with ATRi/RT or ATRi/RT/anti-TIGIT/anti-PD-1 combination therapy. NK cells were depleted in the indicated group using an anti-NK1.1 antibody. Radiation and ATRi dose were increased to 20 Gy in four 5 Gy fractions per day and 75 mg/kg/day for 5 days, respectively. The first ATRi dose was given on the first day of radiotherapy. Combined tumor growth and survival curves from one experiment are shown (six mice/group). (D) SCC7-bearing mice were treated with ATRi and RT at 75 mg/kg/day for 5 days and 24 Gy in three 8 Gy fractions per day over 5 days, respectively. TIGIT and PD-1 blockade antibody treatment was the same as (C). Depletion of NK cells was performed using an anti-Asialo-GM1 antibody in the indicated group. Combined individual tumor growth and survival curves from two independent experiments are shown (10–17 mice/group). Numbers of mice with complete tumor clearance are shown. Results are shown as \pm SEM, one-way analysis of variance followed by Bonferroni's post-t-test except (B) Mann-Whitney U test. Statistical differences between survival groups were determined using the log-rank Mantel-Cox test. Statistical significance: * $p < 0.05$, ** $p < 0.01$, *** $p < 0.001$, **** $p < 0.0001$. ATRi, ataxia telangiectasia and rad3-related inhibitor; IFN- γ , interferon gamma; MFI, mean fluorescence intensity; NK, natural killer.

both anti-TIGIT and anti-PD-1 was necessary, as single antibody treatment failed to exert additional benefits to ATRi/RT.

Next, we checked whether favorable effects from TIGIT/PD-1 immunotherapy resulted in enhanced

NK-cell activity in the TIME. To that end, we compared the effector capacity of tumor NK cells between ATRi/RT and ATRi/RT/anti-TIGIT/anti-PD-1 interventions. NK cells from ATRi/RT/anti-TIGIT/anti-PD-1-treated animals displayed enhanced intensity of CD44, IFN- γ , and

CD107a expression *ex vivo* when compared with ATRi/RT treatment only (figure 5B).

We were interested to assess whether increasing the dose of both radiation and ATRi would further increase the effect of immunotherapy. Using this strategy, mice treated with the ATRi/RT/anti-TIGIT/anti-PD-1 displayed a more pronounced delay in tumor progression when compared with ATRi/RT alone (figure 5C). The efficacy of this treatment regimen was significantly reduced by the depletion of NK cells (figure 5C), indicating the critical contribution of NK cells to therapeutic efficacy. In order to expand the impact of our findings, we tested the same combination treatment in another syngeneic model, namely, SCC7. ATRi/RT treatment induced clear benefits in SCC7 tumor-bearing mice (figure 5D) when immunotherapy alone did not (online supplemental figure S9). Strikingly, all animals in the ATRi/RT/anti-TIGIT/anti-PD-1 combination therapy group achieved complete remission. This can be explained by the increased frequency of tumour-infiltrating CD8 T cells following RT in the SCC7 model when compared with MOC2 (online supplemental figure S10). Tumor control was not achieved in the absence of NK cells (figure 5D and online supplemental figure S11).

Together, these results indicate that the antitumor activity of NK cells can be further enhanced following ATRi/RT by immunotherapies based on TIGIT and PD-1 immune checkpoint blockade.

Combination of radiation and ATRi therapy boosts NK-cell activity in patients with HNSCC

In parallel with our mouse studies, we performed immune profiling on blood samples in patients with HNSCC enrolled in the PATRIOT clinical trial.¹³ As shown in the protocol (online supplemental figure S12), we collected samples at four different timepoints, allowing monitoring of the effect of radiation and ATRi (AZD6738) on NK-cell proportions and activation during treatment. We observed no clear modulation of the frequency of NK cells following therapy (figure 6A). In terms of activation, we noticed a progressive fold change increase in the proportions of 4-1BB and CD95-positive NK cells (figure 6B). The same trend was observed for the marker CD69, although the increase of expression was not sustained toward the end of the treatment (figure 6B). Interestingly, proportions of TIGIT-positive NK cells significantly increased in patients between baseline and prefraction 11 (figure 6C,D). In contrast, expression of PD-1 on NK cells was only increased in one patient and unchanged or decreased for the others (figure 6C).

Taken together, these data indicate that ATRi/RT enhanced NK-cell activation in patients with HNSCC. Furthermore, increased TIGIT expression on NK cells following treatment suggests that therapeutic interventions based on the inhibition of TIGIT signaling might also represent an interesting clinical strategy in humans to boost NK-cell activity following radiotherapy or ATRi/RT combination treatment.

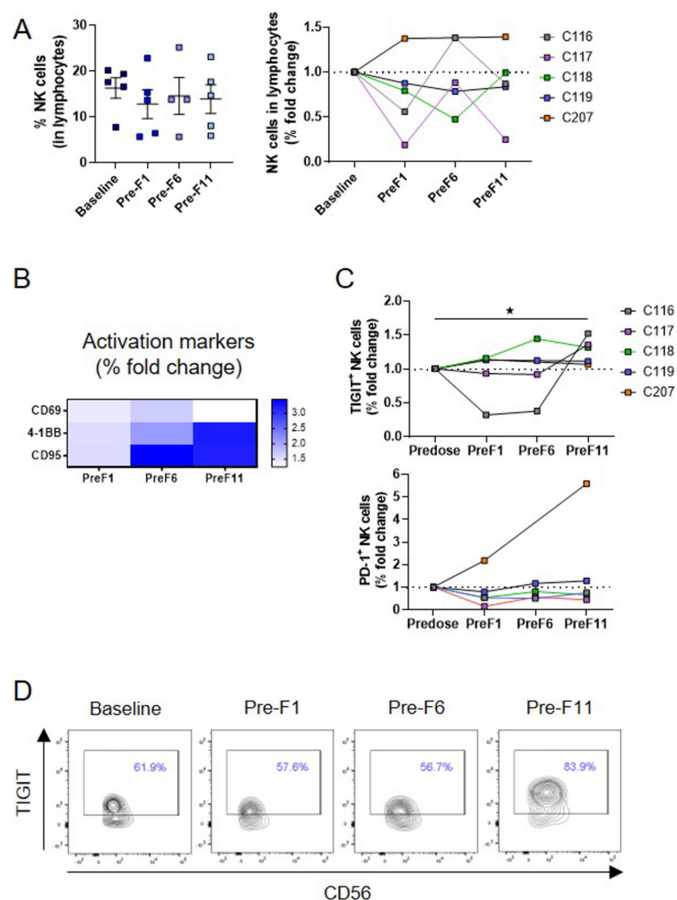


Figure 6 ATRi/RT combination therapy increases activation markers and TIGIT expression on NK cells in patients with HNSCC. Five patients with HNSCC were treated with ATRi/RT combination therapy as described in the Materials and methods section. (A) Proportions of NK cells in blood from patients during ATRi/RT combination therapy shown as percentages related to total CD45⁺ cells (left panel) and percent fold increase (right panel) when compared with baseline (before treatment). (B) heat MAP showing mean % fold increase of CD69, 4-1BB and CD95-positive NK cells during ATRi/RT treatment when compared with baseline. (C) Percent fold increase of TIGIT and PD-1-positive NK cells for each patient during treatment when compared with baseline. (D) Dot plot from one patient illustrating the increase of TIGIT expression on NK cells during the combination treatment. Results are shown as (A, left panel) \pm SEM, (A, right panel; B,C) percent fold change increase. (C) Mann-Whitney U test between baseline and PreF11. Statistical significance: * $p < 0.05$. ATRi, ataxia telangiectasia and rad3-related inhibitor; HNSCC, head and neck squamous cell carcinoma; NK, natural killer.

DISCUSSION

The clinical development of PD-1/PD-L1 ICIs has transformed the management of patients with relapsed/metastatic head and neck cancer. As yet, attempts to introduce ICI earlier in the patient's treatment journey, as part of curative-intent radiotherapy/chemoradiotherapy, have not been successful.^{14–16} Through syngeneic mouse models and analysis of clinical samples, this study points toward a means of combining radiation, ATR-targeted

DDR inhibition, and immunotherapy to improve response and cure rates for patients with head and neck cancer by harnessing NK-cell activity.

A substantial body of research supports radiotherapy and ICIs as a promising therapeutic combination aimed at boosting antitumor immunity.^{10 19–24} The optimal dose, fractionation, and ICI combination regimen to maximize the immunogenic ‘viral mimicry’ response to radiotherapy remains an active area of investigation.^{22 25} This study, building on previous publications,^{8 11} supports the addition of ATR inhibition as a mechanism to enhance the immunogenicity of radiotherapy.

The ATRi ceralasertib in combination with radiotherapy has progressed from phase I¹³ and is now entering a phase II clinical trial in patients with HNSCC undergoing radical radiotherapy (EudraCT# 2020-001034-35). There is an emerging consensus that DDR defects, or the biological effects of DDRi agents are inextricably linked with type-I IFN signaling.^{10 11 26 27} Inhibition of DDR pathways increases micronucleus formation⁸ and levels of cytosolic DNA that drives type I IFN signaling in the TIME through activation of tumor cell cGAS or uptake of DNA by dendritic cells.^{10 28 29} Recent preclinical studies have identified the ability of DDRi agents alone, or paired with radiotherapy, to increase the efficacy of ICIs.^{30–32}

The TIME comprises many different immune cells that exert antitumor or protumor functions.³³ Research on radiotherapy and ICI combinations has focused almost exclusively on CD8 T and dendritic cells. Studies of ICIs alone show intratumoral CD8 T cells are associated with a favorable prognosis,^{34 35} with preclinical studies indicating the importance of CD8 T cells to the efficacy of radiation and DDRi combinations.^{12 36 37} Initial data in the MOC2 model indicated a radiotherapy-induced inflammatory response enhanced by ATRi that was associated with NK cells rather than CD8 T cells. To our knowledge, no previous study has shown the ability of ICIs to harness NK-cell activity in response to radiotherapy/DDRi combination. Therefore, we focused on the therapeutic role of NK cells postradiotherapy/ATRi.

Depletion experiments indicated NK cells were critical for the full efficacy of ATRi/RT. However, as NKT cells also express NK1.1, and NK cells are members of the innate lymphoid cell family, we cannot exclude the involvement of NKT cells or ILC1 cells. Increased NK-cell frequencies in MOC2 tumors by ATRi/RT were associated with enhanced maturation, activating receptor expression, cytokine production, and cytotoxic capacity, mirroring changes in CD8 T cells in analogous therapeutic settings.^{12 36} We were encouraged that many of the phenotypical changes in NK cells presented opportunities to exploit therapeutic approaches currently being developed preclinically and clinically.³⁸

The ability of NK cells to kill tumor cells without prior antigen sensitization makes them attractive targets for immunotherapies,³⁸ and we wished to exploit the vigorous NK-cell activity detected in the TIME following ATRi/RT treatment. It is probable that for some patients,

particularly those with low mutational burdens or loss of neoantigen presentation, an efficacious antitumor T-cell response may not be possible. For these patients, harnessing antitumor NK-cell activity is a potential means to widen response rates to ICIs. Radiation-induced PD-L1 expression was greatly enhanced in the TME by the addition of ATRi/RT. This is in keeping with the emerging consensus that DDRi agents (or DDR defects) drive type I IFN signaling and, subsequently, PD-L1 expression.^{10 11 26 27}

Despite this high PD-L1 signal, anti-PD-1 antibodies alone did not augment the therapeutic efficacy of ATRi/RT. This diversity of responses to anti-PD-1 immunotherapy between mouse models reflects the conclusions from clinical investigations, where overall response rates in patients are still low and intensive research is focused on alternative ICI approaches.

One such approach is dual-ICI blockade. Among all the immune checkpoints investigated in our study, only TIGIT showed enhanced surface expression on NK cells in response to ATRi/RT. TIGIT upregulation was most evident on mature CD11b⁺/CD27[−] NK cells. The TIGIT ligand, PVR (CD155), was also increased on cancer cells, monocytes and macrophages. Interestingly, TIGIT was not flagged as a target of interest in our global RNA-seq analysis, which showed a significant decrease of total *Tigit* transcripts in MOC2 tumors. Flow cytometric data indicated stable surface TIGIT expression in CD8 T cells and reduced expression in CD4 T cells, contrasting with elevation on NK cells.

A number of anti-TIGIT antibodies are under clinical evaluation in patients with cancer.³⁹ Interference with TIGIT signaling in NK cells has recently been shown to be particularly relevant for antitumor immunity.^{40 41} Having said that, in MOC2-bearing mice treated with ATRi/RT, TIGIT blockade alone, like PD-1 blockade alone, was insufficient to enhance therapeutic outcomes. Recent investigations have highlighted the potential of targeting TIGIT, with or as an alternative to PD-1 axis blockade.^{42 43} Grapin and colleagues reported that only dual anti-PD-1 and anti-TIGIT blockade was effective in delivering additional antitumor control in combination with radiotherapy in the CT-26 model.⁴⁴ In our study, the prominent expression of PD-L1 observed on cancer and myeloid cells following ATRi/RT provided a strong rationale for blockade of the PD-1/PD-L1 axis, with PVR expression and the NK cell-specific levels of TIGIT providing a strong rationale for concomitant blockade of the TIGIT signaling axis. Subsequently, dual PD-1/TIGIT blockade was confirmed to enhance NK cell-mediated tumor control in combination with ATRi/RT. Considering levels of surface expression of both PVR and PD-L1 on cancer and myeloid cells following ATRi/RT, the effect of combined TIGIT and PD-1 blockade is likely due to the disruption of the binding of those receptors to their ligands, PVR, and PD-L1. However, we cannot rule out the possibility that other TIGIT and PD-1 ligands, such as Nectin-2 and PD-L2, play a role in the effects we observed.

NK-cell activity can be associated with a positive prognosis in patients with human cancer,^{45 46} particularly

in HNSCC.² Analysis of clinical samples from patients receiving radiation and ATRi treatment indicated an increase in NK-cell surface expression of activation markers after combined ATRi/RT, in line with our preclinical data. Of note, the presence of mature CD56^{dim} NK cells, a subpopulation with increased cytolytic activities,⁴⁷ was correlated with improved survival in patients with HNSCC.² We found that TIGIT was generally highly expressed on blood NK cells, which has been reported previously in patients with HNSCC.⁴⁰ TIGIT signaling impairs human NK-cell cytotoxicity toward tumor cells.⁴⁸ Due to increased frequencies of NK cells expressing TIGIT following combined ATRi/RT, it is tempting to hypothesize that those patients might derive therapeutic benefit from additional treatments based on anti-TIGIT and/or anti-PD-1-blocking antibodies.

To conclude, our study has demonstrated the potential to exploit NK-cell activity to improve radiation and DDRi therapeutic effects in head and neck cancer. This approach has the potential to be translated to clinical studies, with particular relevance to poorly immunogenic tumors. Such a strategy might provide an attractive alternative to traditional T cell-based approaches, with the potential to expand the number of patients responsive to cancer immunotherapy in the near future.

Contributors ECP, KJH, MM, and MTD contributed to the conception and design of the research as well as in writing the manuscript; ECP, MM, MTD, LG, GB, EC-R, HB, HW, GB, and JK performed the experiments and acquired data; ECP, KJH, MM, MTD, MP, PN, JH, HG, SS, and AAM contributed to the analysis and interpretation of the data. MM and PN provided support for bioinformatics analysis; MTD, PN, HS, IL, DN, and JG contributed to the collection and supply of clinical samples. JH, HG, and SS contributed to the supply of reagents. KJH is the guarantor, senior author and provided funding for the project. All authors read and approved the final manuscript.

Funding This study was supported by RM/ICR NIHR Biomedical Research Centre Center (KH), Rosetrees Trust (EP, MD, and KH); grant numbers M48 and M444), Cancer Research United Kingdom (MD, AM, and KH) and The Oracle Cancer Trust (EP, MM, MP, EC-R, and KH).

Competing interests None declared.

Patient consent for publication Not applicable.

Ethics approval This study involves human subjects and was approved by NRES Committee London – City and EastREC (ref: 14/LO/0465), and was conducted in accordance with protocol requirements, Good Clinical Practice, and the guiding principles of the Declaration of Helsinki. All subjects provided written informed consent to participate in the study before taking part. The protocol was reviewed by the local ethics committee.

Provenance and peer review Not commissioned; externally peer reviewed.

Data availability statement Data are available upon reasonable request.

Supplemental material This content has been supplied by the author(s). It has not been vetted by BMJ Publishing Group Limited (BMJ) and may not have been peer-reviewed. Any opinions or recommendations discussed are solely those of the author(s) and are not endorsed by BMJ. BMJ disclaims all liability and responsibility arising from any reliance placed on the content. Where the content includes any translated material, BMJ does not warrant the accuracy and reliability of the translations (including but not limited to local regulations, clinical guidelines, terminology, drug names and drug dosages), and is not responsible for any error and/or omissions arising from translation and adaptation or otherwise.

Open access This is an open access article distributed in accordance with the Creative Commons Attribution Non Commercial (CC BY-NC 4.0) license, which permits others to distribute, remix, adapt, build upon this work non-commercially, and license their derivative works on different terms, provided the original work is

properly cited, appropriate credit is given, any changes made indicated, and the use is non-commercial. See <http://creativecommons.org/licenses/by-nc/4.0/>.

ORCID iDs

Emmanuel C Patin <http://orcid.org/0000-0001-5390-5733>
 Pablo Nenclares <http://orcid.org/0000-0002-1750-3179>
 Malin Pedersen <http://orcid.org/0000-0003-1887-733X>
 Martin McLaughlin <http://orcid.org/0000-0002-9739-7133>
 Kevin J Harrington <http://orcid.org/0000-0002-6014-348X>

REFERENCES

- Sung H, Ferlay J, Siegel RL, *et al*. Global cancer statistics 2020: GLOBOCAN estimates of incidence and mortality worldwide for 36 cancers in 185 countries. *CA Cancer J Clin* 2021;71:209–49.
- Mandal R, Şenbabaoğlu Y, Desrichard A, *et al*. The head and neck cancer immune landscape and its immunotherapeutic implications. *JCI Insight* 2016;1:e89829.
- Nickoloff JA, Boss M-K, Allen CP, *et al*. Translational research in radiation-induced DNA damage signaling and repair. *Transl Cancer Res* 2017;6:S875–91.
- Pilié PG, Tang C, Mills GB, *et al*. State-Of-The-Art strategies for targeting the DNA damage response in cancer. *Nat Rev Clin Oncol* 2019;16:81–104.
- Lecona E, Fernandez-Capetillo O. Targeting ATR in cancer. *Nat Rev Cancer* 2018;18:586–95.
- Yap TA, Tan DSP, Terbuch A, *et al*. First-In-Human trial of the oral ataxia telangiectasia and Rad3-related (ATR) inhibitor Bay 1895344 in patients with advanced solid tumors. *Cancer Discov* 2021;11:80–91.
- Thomas A, Takahashi N, Rajapakse VN, *et al*. Therapeutic targeting of ATR yields durable regressions in small cell lung cancers with high replication stress. *Cancer Cell* 2021;39:566–79.
- Dillon MT, Barker HE, Pedersen M, *et al*. Radiosensitization by the ATR inhibitor AZD6738 through generation of acentric micronuclei. *Mol Cancer Ther* 2017;16:25–34.
- Harding SM, Benci JL, Irianto J, *et al*. Mitotic progression following DNA damage enables pattern recognition within micronuclei. *Nature* 2017;548:466–70.
- McLaughlin M, Patin EC, Pedersen M, *et al*. Inflammatory microenvironment remodelling by tumour cells after radiotherapy. *Nat Rev Cancer* 2020;20:203–17.
- Dillon MT, Bergerhoff KF, Pedersen M, *et al*. Atr inhibition potentiates the radiation-induced inflammatory tumor microenvironment. *Clin Cancer Res* 2019;25:3392–403.
- Vendetti FP, Karukonda P, Clump DA, *et al*. Atr kinase inhibitor AZD6738 potentiates CD8+ T cell-dependent antitumor activity following radiation. *J Clin Invest* 2018;128:3926–40.
- Dillon MT, Boylan Z, Smith D, *et al*. Patriot: a phase I study to assess the tolerability, safety and biological effects of a specific ataxia telangiectasia and Rad3-related (ATR) inhibitor (AZD6738) as a single agent and in combination with palliative radiation therapy in patients with solid tumours. *Clin Transl Radiat Oncol* 2018;12:16–20.
- Ferris RL, Blumenschein G, Fayette J, *et al*. Nivolumab for recurrent squamous-cell carcinoma of the head and neck. *N Engl J Med* 2016;375:1856–67.
- Burtneß B, Harrington KJ, Greil R, *et al*. Pembrolizumab alone or with chemotherapy versus cetuximab with chemotherapy for recurrent or metastatic squamous cell carcinoma of the head and neck (KEYNOTE-048): a randomised, open-label, phase 3 study. *Lancet* 2019;394:1915–28.
- Cohen EEW, Soulières D, Le Tourneau C, *et al*. Pembrolizumab versus methotrexate, docetaxel, or cetuximab for recurrent or metastatic head-and-neck squamous cell carcinoma (KEYNOTE-040): a randomised, open-label, phase 3 study. *The Lancet* 2019;393:156–67.
- Lee NY, Ferris RL, Psyrrri A, *et al*. Avelumab plus standard-of-care chemoradiotherapy versus chemoradiotherapy alone in patients with locally advanced squamous cell carcinoma of the head and neck: a randomised, double-blind, placebo-controlled, multicentre, phase 3 trial. *Lancet Oncol* 2021;22:450–62.
- Harrington KJ, Ferris RL, Blumenschein G, *et al*. Nivolumab versus standard, single-agent therapy of investigator's choice in recurrent or metastatic squamous cell carcinoma of the head and neck (CheckMate 141): health-related quality-of-life results from a randomised, phase 3 trial. *Lancet Oncol* 2017;18:1104–15.
- Dovedi SJ, Cheadle EJ, Popple AL, *et al*. Fractionated radiation therapy stimulates antitumor immunity mediated by both resident and infiltrating polyclonal T-cell populations when combined with PD-1 blockade. *Clin Cancer Res* 2017;23:5514–26.

- 20 Formenti SC, Rudqvist N-P, Golden E, *et al.* Radiotherapy induces responses of lung cancer to CTLA-4 blockade. *Nat Med* 2018;24:1845–51.
- 21 Antonia SJ, Villegas A, Daniel D, *et al.* Overall survival with Durvalumab after chemoradiotherapy in stage III NSCLC. *N Engl J Med* 2018;379:2342–50.
- 22 Vanpouille-Box C, Alard A, Aryankalayil MJ, *et al.* Dna exonuclease TREX1 regulates radiotherapy-induced tumour immunogenicity. *Nat Commun* 2017;8:15618.
- 23 Weichselbaum RR, Liang H, Deng L, *et al.* Radiotherapy and immunotherapy: a beneficial liaison? *Nat Rev Clin Oncol* 2017;14:365–79.
- 24 Hou Y, Liang HL, Yu X, *et al.* Radiotherapy and immunotherapy converge on elimination of tumor-promoting erythroid progenitor cells through adaptive immunity. *Sci Transl Med* 2021;13. doi:10.1126/scitranslmed.abb0130. [Epub ahead of print: 24 02 2021].
- 25 Dewan MZ, Galloway AE, Kawashima N, *et al.* Fractionated but not single-dose radiotherapy induces an immune-mediated abscopal effect when combined with anti-CTLA-4 antibody. *Clin Cancer Res* 2009;15:5379–88.
- 26 Chabanon RM, Muirhead G, Krastev DB, *et al.* Parp inhibition enhances tumor cell-intrinsic immunity in ERCC1-deficient non-small cell lung cancer. *J Clin Invest* 2019;129:1211–28.
- 27 Parkes EE, Walker SM, Taggart LE, *et al.* Activation of STING-dependent innate immune signaling by S-phase-specific DNA damage in breast cancer. *J Natl Cancer Inst* 2017;109. doi:10.1093/jnci/djw199. [Epub ahead of print: 05 10 2016].
- 28 Sen T, Rodriguez BL, Chen L, *et al.* Targeting DNA damage response promotes antitumor immunity through STING-mediated T-cell activation in small cell lung cancer. *Cancer Discov* 2019;9:646–61.
- 29 Woo S-R, Fuertes MB, Corrales L, *et al.* Sting-Dependent cytosolic DNA sensing mediates innate immune recognition of immunogenic tumors. *Immunity* 2014;41:830–42.
- 30 Patel P, Sun L, Robbins Y, *et al.* Enhancing direct cytotoxicity and response to immune checkpoint blockade following ionizing radiation with Wee1 kinase inhibition. *Oncoimmunology* 2019;8:e1638207.
- 31 Zhang Q, Green MD, Lang X, *et al.* Inhibition of ATM increases interferon signaling and sensitizes pancreatic cancer to immune checkpoint blockade therapy. *Cancer Res* 2019;79:3940–51.
- 32 Sheng H, Huang Y, Xiao Y, *et al.* Atr inhibitor AZD6738 enhances the antitumor activity of radiotherapy and immune checkpoint inhibitors by potentiating the tumor immune microenvironment in hepatocellular carcinoma. *J Immunother Cancer* 2020;8:e000340.
- 33 Fridman WH, Pagès F, Sautès-Fridman C, *et al.* The immune contexture in human tumours: impact on clinical outcome. *Nat Rev Cancer* 2012;12:298–306.
- 34 Farhood B, Najafi M, Mortezaee K. CD8⁺ cytotoxic T lymphocytes in cancer immunotherapy: A review. *J Cell Physiol* 2019;234:8509–21.
- 35 Leclerc M, Voilin E, Gros G, *et al.* Regulation of antitumour CD8 T-cell immunity and checkpoint blockade immunotherapy by neuropilin-1. *Nat Commun* 2019;10:3345.
- 36 Hanoteau A, Newton JM, Krupar R, *et al.* Tumor microenvironment modulation enhances immunologic benefit of chemoradiotherapy. *J Immunother Cancer* 2019;7:10.
- 37 Luo R, Firat E, Gaedicke S, *et al.* Cisplatin facilitates radiation-induced Abscopal effects in conjunction with PD-1 checkpoint blockade through CXCR3/CXCL10-Mediated T-cell recruitment. *Clin Cancer Res* 2019;25:7243–55.
- 38 Valipour B, Velaei K, Abedelahi A, *et al.* Nk cells: an attractive candidate for cancer therapy. *J Cell Physiol* 2019;234:19352–65.
- 39 Solomon BL, Garrido-Laguna I. Tigit: a novel immunotherapy target moving from bench to bedside. *Cancer Immunol Immunother* 2018;67:1659–67.
- 40 Wu L, Mao L, Liu J-F, *et al.* Blockade of TIGIT/CD155 signaling reverses T-cell exhaustion and enhances antitumor capability in head and neck squamous cell carcinoma. *Cancer Immunol Res* 2019;7:1700–13.
- 41 Zhang Q, Bi J, Zheng X, *et al.* Blockade of the checkpoint receptor TIGIT prevents NK cell exhaustion and elicits potent anti-tumor immunity. *Nat Immunol* 2018;19:723–32.
- 42 Hung AL, Maxwell R, Theodoros D, *et al.* Tigit and PD-1 dual checkpoint blockade enhances antitumor immunity and survival in GBM. *Oncoimmunology* 2018;7:e1466769.
- 43 Johnston RJ, Comps-Agrar L, Hackney J, *et al.* The immunoreceptor TIGIT regulates antitumor and antiviral CD8(+) T cell effector function. *Cancer Cell* 2014;26:923–37.
- 44 Grapin M, Richard C, Limagne E, *et al.* Optimized fractionated radiotherapy with anti-PD-L1 and anti-TIGIT: a promising new combination. *J Immunother Cancer* 2019;7:160.
- 45 Ben-Shmuel A, Biber G, Barda-Saad M. Unleashing natural killer cells in the tumor Microenvironment-The next generation of immunotherapy? *Front Immunol* 2020;11:275.
- 46 Imai K, Matsuyama S, Miyake S, *et al.* Natural cytotoxic activity of peripheral-blood lymphocytes and cancer incidence: an 11-year follow-up study of a general population. *Lancet* 2000;356:1795–9.
- 47 Moretta L. Dissecting CD56dim human NK cells. *Blood* 2010;116:3689–91.
- 48 Stanietsky N, Simic H, Arapovic J, *et al.* The interaction of TIGIT with PVRL2 inhibits human NK cell cytotoxicity. *Proc Natl Acad Sci U S A* 2009;106:17858–63.

Harnessing radiotherapy-induced NK-cell activity by combining DNA damage-response inhibition and immune checkpoint blockade

Supplementary material

Methods

Flow cytometry antibodies

Monoclonal antibodies against mouse CD45 (clone 30-F11 PE-, AF700- or BUV805-conjugated), human CD45 (clone HI30, BV650-conjugated), mouse CD3 (clone 17A2, Pacific Blue-, BV650-, PerCp Cy5.5 or BUV563-conjugated), human CD3 (clone HIT3a, AF700-conjugated), mouse CD4 (clone RMA4-5, v500- or BUV496-conjugated), mouse CD8 α (clone 53-6.7, BV650-, PE-CF594-, PE-Cy7- or BV570-conjugated), mouse CD8 β (clone 53-5.8, FITC-conjugated), mouse NK1.1 (clone PK136, APC-, BV421- or PD-Dazzle 594-conjugated), mouse NKp46 (clone 29A1.4, APC-, PeCy7- or BUV737-conjugated), human CD56 (clone HCD56, PE-dazzle 594-conjugated), mouse TCR δ (clone GL3, PerCp Cy5.5-conjugated), mouse CD19 (clone 6D5, FITC- or APC-conjugated), mouse B220 (clone RA3-6B2, FITC- or PerCp Cy5.5-conjugated), mouse CD44 (clone IM7, Pacific Blue-, FITC- or BUV379-conjugated), mouse FoxP3 (clone FJK-16s, eFluor 450-conjugated), mouse CD25 (clone PC61, BV650- or APC- conjugated), mouse IFN- γ (clone XM61.2, AF488- or BV750-conjugated), mouse TNF- α (clone MP6-XT22, AF700-conjugated), mouse/human Granzyme B (clone GB11, AF647-conjugated), mouse CD69 (clone H1.2F3, FITC-, PE or PE-Cy7-conjugated), human CD69 (clone FN50, APC-Cy7-conjugated), human CD95 (clone DX2, APC-Cy7-conjugated), mouse Ki67 (clone 16A8, AF488- or PE-conjugated), mouse KLRG1 (clone 2F1/KLRG1, FITC-conjugated), mouse CD107a antibody (clone 1D4B, PE- or BUV379-conjugated), mouse CTLA-4 (clone UC10-4B9, PE-conjugated), mouse NKG2D (clone CX5, FITC- and PE-conjugated), mouse CD96 (TACTILE) (clone 3.3, PE-conjugated), mouse CD62L (clone MEL-14, PE-dazzle 594- or AF700-conjugated), mouse CD27 (clone LG.3410, PE-dazzle 594- or PE-Cy7-conjugated), mouse LAG-3 (clone C9B7W, FITC-conjugated), mouse VISTA (clone M1H63, APC-conjugated), mouse TIM-3 (clone RMT3-23, APC-conjugated), mouse TIGIT (clone GIGD7, PerCp eFluor 710-conjugated), human TIGIT (clone MBSA43, PerCp eFluor 710-conjugated), mouse PD-1 (clone 29F.1A12, PE-Cy7-conjugated), human PD-1 (clone EH12.EH7, PE-conjugated), mouse NKG2A (clone 16A11, PE- or PE-Cy7-conjugated), mouse 4-1BB (clone 17B5, APC-conjugated), human 4-1BB (clone 4B4-1, APC-conjugated), mouse F4/80 (clone BM8, Pacific Blue-conjugated), mouse Ly6G (clone 1A8, BV510-conjugated), mouse CD11b (clone M1/70, BV650- or FITC-conjugated), mouse Ly6C (clone HK1.4, FITC- or APC-conjugated), mouse CD11c (clone N418, FITC-, PerCp Cy5.5- or PE-Cy7-conjugated), mouse EpCAM

(clone G8.8, FITC- or APC-conjugated), mouse CD206 (clone C063C2, PE-dazzle 594-conjugated), mouse PD-L1 (clone 10F.9G2, PerCp Cy5.5-conjugated), mouse MHCII (clone M5/114.15.2, AF700-conjugated), mouse CD155 (PVR) (clone TX56, PE-Cy7-conjugated) and appropriated isotype controls were purchased from BioLegend, BD Pharmingen and Thermofisher Scientific. Fixable Viability Dye eFluor 780 was purchased from Thermofisher Scientific and incubated concomitantly to surface staining antibodies.

Supplementary figures

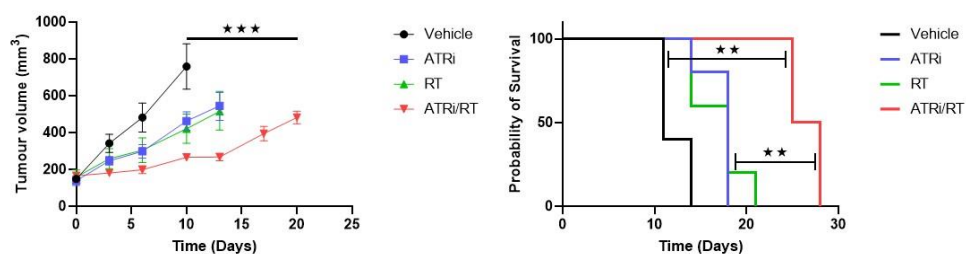


Figure S1. ATRi potentiates RT-mediated anti-tumour response in the AT84 model. 2.10^6 AT84 cells were injected subcutaneously into C3H mice. When tumours reached 80-200 mm³, mice were treated with ATRi (25 mg/kg daily for 7 days) and RT (8 Gy in four 2 Gy daily fractions) at time as indicated. Primary tumour growth was monitored every 3 to 4 days. Combined tumour growth and survival curves from one experiment are shown (5 mice/group). Results are shown as \pm SEM, one-way ANOVA followed by Bonferroni's post T test. Statistical differences between survival groups were determined using the Log-rank Mantel Cox test. Statistical significance: ** $p < 0.01$; *** $p < 0.001$.

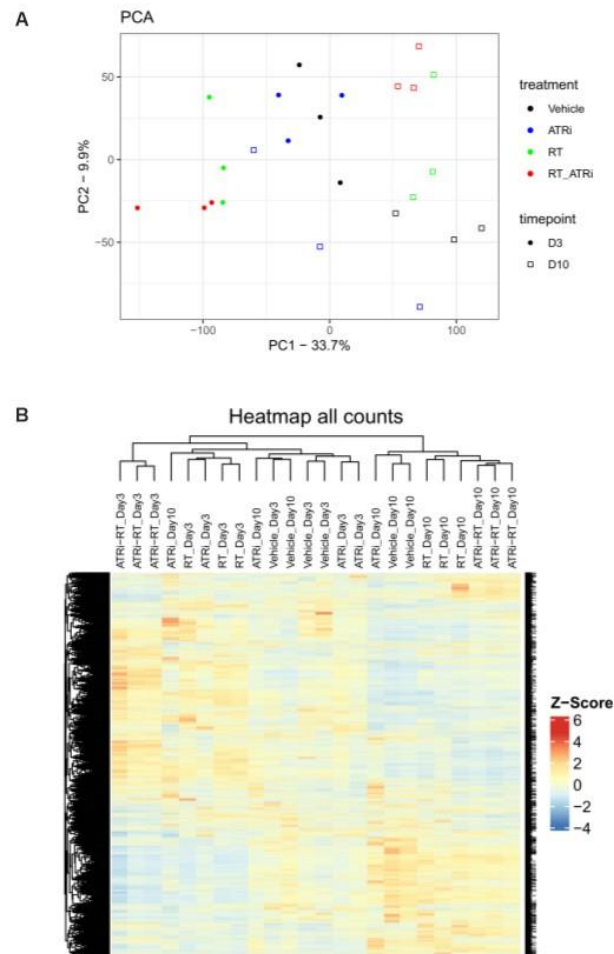


Figure S2. Principal component analysis and heatmap clustering of RNA-seq data. (A) Principal component analysis was performed on RNA-seq data indicating the clustering of samples by timepoint and treatment. (B) A heatmap showing non-hierarchical clustering performed on both samples and genes, including all genes, not just those differentially expressed. Sample clustering was strongly linked to both treatment and timepoint.

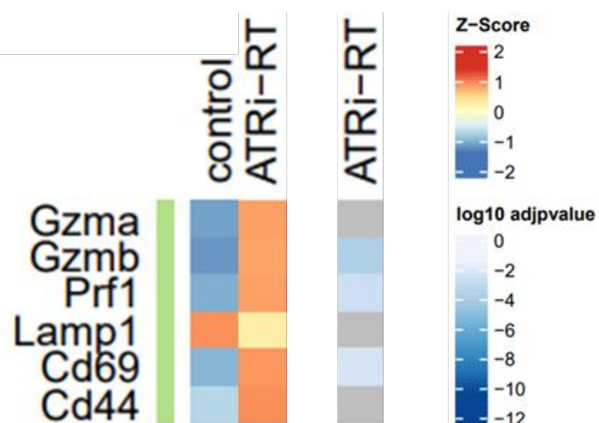


Figure S3. MOC2 RNAseq activation marker analysis at Day 10. Heatmaps corresponding to activation markers, Data shown are z-scores of log₂ transformed normalised counts at Day 10 for the treatment conditions shown. These data are plotted alongside log₁₀ adjusted *p*-value for each gene calculated from DEG analysis using DESeq2. Non-significant adjusted *p*-values > 0.05 are indicated as grey.

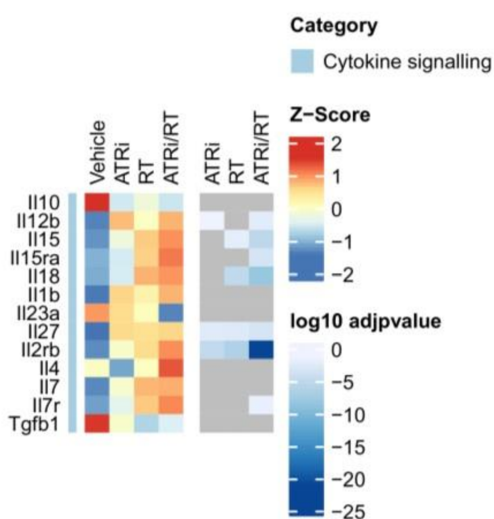


Figure S4. MOC2 RNAseq cytokine signalling analysis. Heatmaps corresponding to cytokine signalling, Data shown are z-scores of log₂ transformed normalised counts at Day 3 for the treatment conditions shown. These data are plotted alongside log₁₀ adjusted *p*-value for each gene calculated from DEG analysis using DESeq2. Non-significant adjusted *p*-values > 0.05 are indicated as grey.

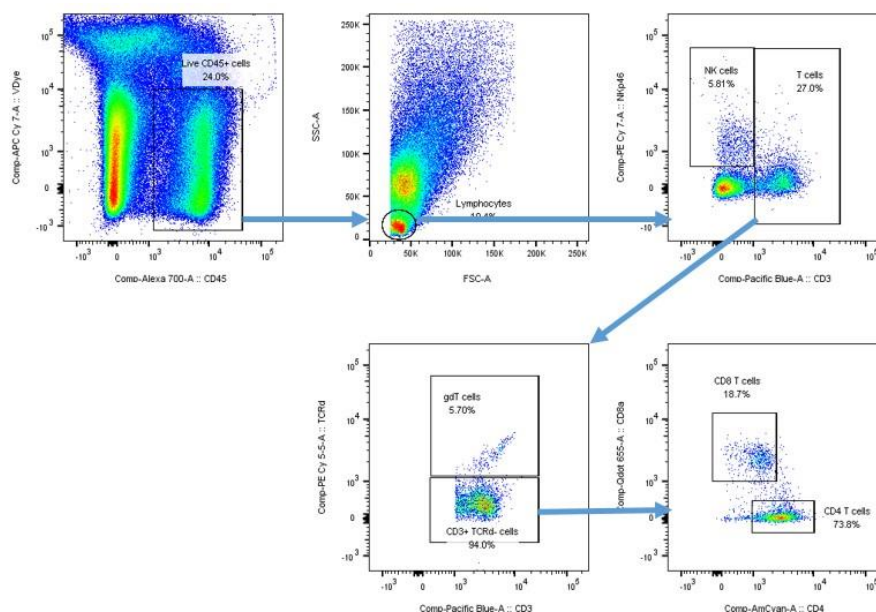


Figure S5. Flow cytometry gating strategy for immune profiling. The figure depicts an example of the gating strategy used in MOC-2 tumours. From the total CD45⁺ live population, lymphocytes were gated using SSC/FSC. NK cells were then gated as CD3⁻ NK1.1⁺ and T cells as CD3⁺ cells. From the T cell population, $\gamma\delta$ T cells were gated as CD3⁺ TCRd⁺ and the conventional CD8 and CD4 T cells as CD3⁺ TCRd⁻CD8⁺ and CD3⁺ TCRd⁻CD4⁺, respectively.

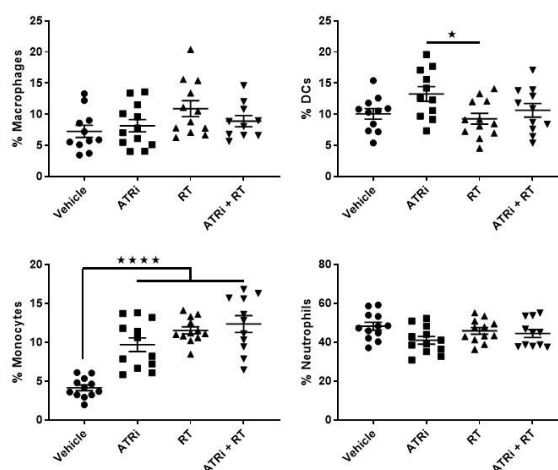


Figure S6. Frequencies of myeloid cell populations in MOC-2 tumours following ATRi/RT combination treatment. MOC-2 tumour-bearing mice were treated with ATRi/RT combination therapy as previously described. Tumours were collected one day after the last ATRi dose for flow cytometry analysis. Macrophages (CD11b⁺F4/80⁺Ly6C^{low}CD11c/MHCII^{low}), DCs (CD11c/MHCII^{high}),

monocytes (CD11b⁺Ly6C^{high}CD11c/MHCII^{low}) and neutrophils (CD11b⁺Ly6G⁺F4/80⁺Ly6C^{med}CD11c/MHCII^{low}) proportions in total live CD45⁺ cells were compared between each group. Combined percentages from two independent experiments are shown (12 mice/group). Results are shown as \pm SEM, one-way ANOVA followed by Bonferroni's post T test. Statistical significance: * $p < 0.05$; **** $p < 0.0001$.

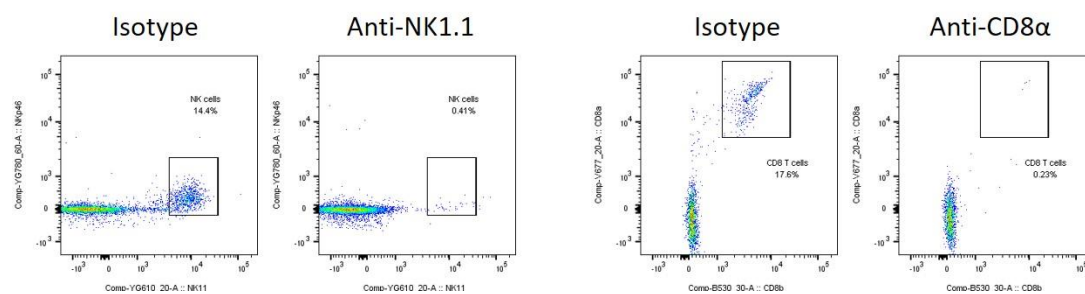


Figure S7. Verification of NK cells and CD8 T cells depletion in tumours during ATRi/RT combination treatment. MOC-2 tumour-bearing mice were treated with ATRi/RT combination therapy. NK cells or CD8 T cells were depleted using an anti-NK1.1 or anti-CD8 α antibody, respectively. Dot plot examples for one tumour in each group are shown. NK cells were gated as CD3⁻NK1.1⁺NKp46⁺ and CD8 T cells as CD3⁺CD8 α ⁺CD8 β ⁺.

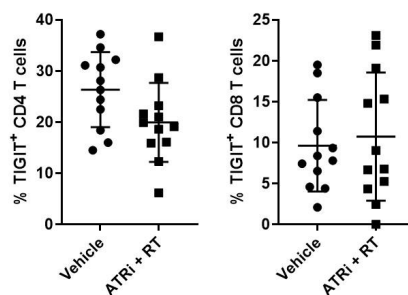


Figure S8. TIGIT expression on conventional T cells following ATRi/RT combination therapy. Percentages of MOC-2 tumour CD4 and CD8 T cells expressing TIGIT following ATRi/RT combination therapy as previously described (12 mice/group).

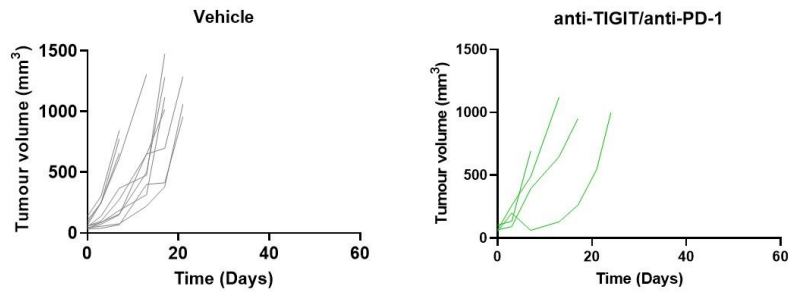


Figure S9. Combined blockade of TIGIT and PD-1 does not lead to tumour clearance in the SCC7 model. SCC7-bearing mice were treated with anti-TIGIT and anti-PD-1 antibodies twice weekly for three weeks. Combined individual tumour growths are shown (10-4 mice/group).

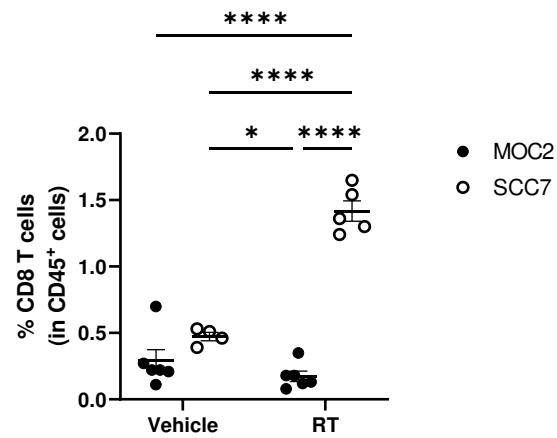


Figure S10. Frequencies of tumour-infiltrating CD8 T cells following RT. Percentages of MOC-2 tumour CD8 T cells following RT as previously described (4-6 mice/group).

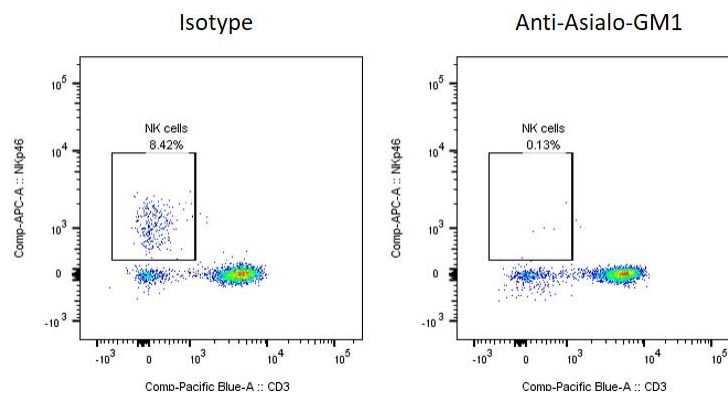


Figure S11. Verification of NK cells depletion in blood during ATRi/RT combination treatment. SCC7 tumour-bearing mice were treated with ATRi/RT combination therapy. NK cells were depleted using an anti-Asialo-GM1. Dot plot examples for one mouse in each group are shown. NK cells were gated as CD3⁻NKp46⁺.

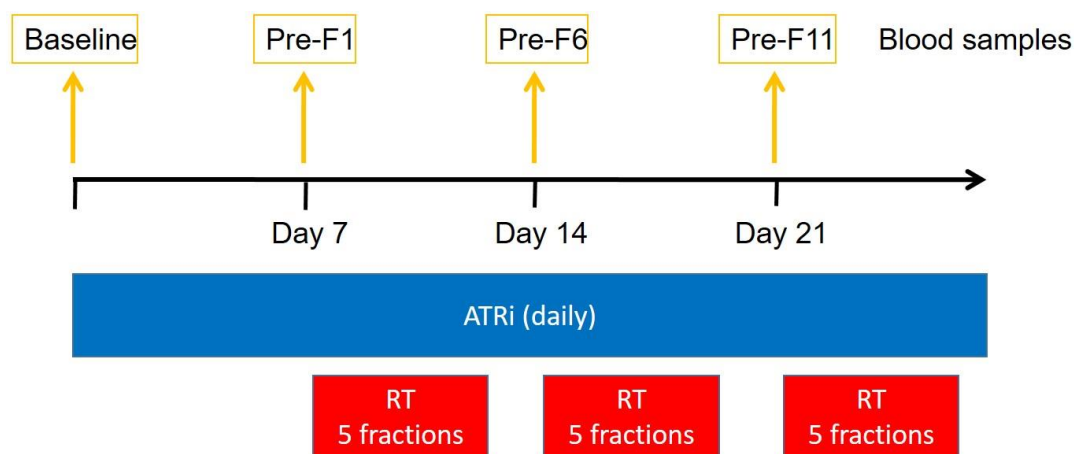
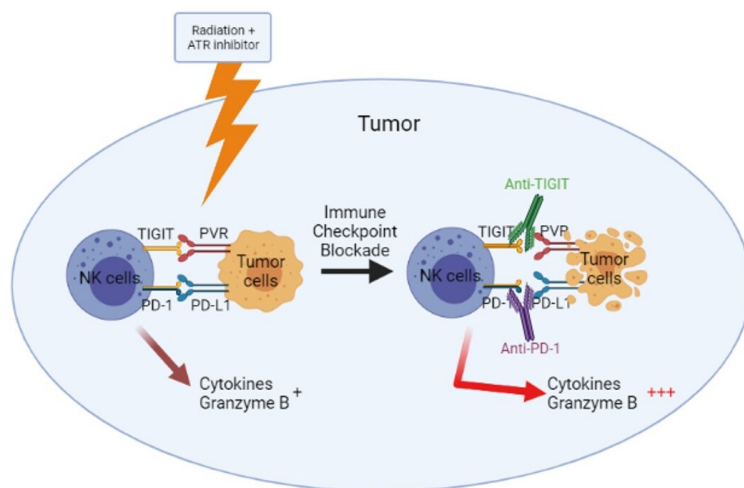


Figure S12. PATRIOT clinical trial protocol. HSNCC patients enrolled in the clinical trial were treated following the protocol as described in the figure. Radiotherapy was administered daily, 2 Gy per fraction, Monday-Friday. A total of up to 30 Gy in 15 fractions was administered. ATRi was given orally for 3-7 days before the start of radiotherapy, during radiotherapy, and for 2 days after. Blood was taken before ATRi dosing, before fraction 1, before fraction 6, and before fraction 11.

Harnessing radiotherapy-induced NK-cell activity by combining DNA damage-response inhibition and immune checkpoint blockade



Authors

Emmanuel C Patin, Magnus T Dillon, Pablo Nenclares, Lorna Grove, Heba Soliman, Isla Leslie, Davina Northcote, Galabina Bozhanova, Eva Crespo-Rodriguez, Holly Baldock, Harriet Whittock, Gabby Baker, Joan Kyula, Jeane Guevara, Alan A. Melcher, James Harper, Hormas Ghadially, Simon Smith, Malin Pedersen, Martin McLaughlin and Kevin J Harrington

Correspondence

emmanuel.patin@icr.ac.uk

In brief

Harnessing NK-cell activity, by combining DNA damage-response inhibition and dual immune TIGIT and PD-1 blockade, is shown to have the potential to improve radiotherapy responses in head and neck cancer